arXiv:nucl-ex/9811007 v2 18 Nov 1998

LBNL–42524
November, 1998

Two–Photon Physics in Nucleus-Nucleus Collisions at RHIC

Joakim Nystrand and Spencer Klein

Lawrence Berkeley National Laboratory,
Berkeley, California 94720, U.S.A.
E-mail: JINystrand@lbl.gov, SRKlein@lbl.gov

and

the STAR Collaboration [1]

Invited talk presented at Workshop on Photon Interactions and the Photon Structure, Lund, Sweden, September 10–13, 1998

Abstract

Ultra–relativistic heavy–ions carry strong electromagnetic and nuclear fields. Interactions between these fields in peripheral nucleus–nucleus collisions can probe many interesting physics topics. This presentation will focus on coherent two–photon and photonuclear processes at RHIC. The rates for these interactions will be high. The coherent coupling of all the protons in the nucleus enhances the equivalent photon flux by a factor Z^2 up to an energy of ~ 3 GeV. The plans for studying coherent interactions with the STAR experiment will be discussed. Experimental techniques for separating signal from background will be presented.

1 The Relativistic Heavy-ion Collider (RHIC) and the STAR Experiment

The Relativistic Heavy-Ion Collider (RHIC), which is now under construction at the Brookhaven National Laboratory, is designed to accelerate protons and nuclei (A=1–197) to energies of 100 – 250 A GeV [1]. The center-of-mass collision energies will be an order of magnitude higher than has previously been available for heavy nuclei. Some of the possible beams, with corresponding beam energies and luminosities, are listed in Table 1. RHIC will begin operation in 1999.

STAR (Solenoidal Tracker at RHIC) is one of two large experiments at RHIC[2]. STAR is primarily designed to study hadronic observables over a wide region of phase space. The main detector is a large, cylindrical Time Projection Chamber (TPC), which is placed inside a 0.5 T solenoidal magnet. Tracks of charged particles produced in the interactions will be reconstructed in the TPC, and the particle momenta will be determined from the curvature in the magnetic field. Information on energy loss in the TPC gas may be used

[1]The STAR Collaboration list can be found (under "organization") at:
http://rsgi01.rhic.bnl.gov/star/starlib/doc/www/star.html

Projectile	Z	A	Kinetic Energy [A GeV]	Lorentz factor, γ	Luminosity [$\mathrm{cm^{-2}\ s^{-1}}$]
p	1	1	251	268	$1.4 \cdot 10^{31}$
O	8	16	125	135	$9.8 \cdot 10^{28}$
Si	14	28	125	135	$4.4 \cdot 10^{28}$
Cu	29	63	115	126	$9.5 \cdot 10^{27}$
I	53	127	104	113	$2.7 \cdot 10^{27}$
Au	79	197	100	108	$2.0 \cdot 10^{26}$

Table 1: Possible beam projectiles and maximum energies and luminosities at RHIC, from the RHIC conceptual design report[1].

to identify low–momentum particles. The main TPC roughly covers the pseudorapidity range $|\eta| < 2.0$ ($\eta = -\tan(\theta/2)$, where θ is the polar emission angle).

Other detectors in STAR are the forward TPCs (FTPC), the silicon vertex tracker (SVT), and the electromagnetic calorimeter (EMC). The forward TPCs will complement the main TPC by detecting charged particles in the range $2.5 \leq |\ \eta\ | \leq 3.75$. A Time–of–Flight (TOF) system and a Ring–Imaging Cherenkov (RICH) detector have been proposed and would provide improved particle identification at high momenta. Figure 1 shows a picture of STAR.

STAR will have a flexible multi–level trigger. In the lower trigger levels, the trigger information will be provided by the central trigger barrel (CTB) and the TPC anode wires, operating as wire chambers. The CTB consists of 240 scintillators covering $|\eta| < 1$; the TPC anode wires will provide multiplicity information in the range $1 < |\eta| < 2$. In the highest trigger level TPC tracking information will also be available. In addition, zero–degree calorimeters along the beam lines on either side of the experiment (for detection of neutrons in nuclear breakup) are used for triggering.

Section 5 will discuss the experimental techniques for studying coherent interactions within STAR. The analyses presented there will be based on a year 1 configuration of STAR consisting of the main TPC, forward TPCs, CTB, and the TPC anode wire read–out. Without the EMC, only final states consisting exclusively of charged particles will be considered.

2 Coherent Nuclear Interactions

Coherent nuclear interactions are defined as reactions between the fields of the nuclei, whereby the fields couple coherently to all the nucleons. The nuclei do not directly participate in these interactions, but act as sources of fields. In the reactions,

$$A + A \rightarrow A + A + X\ , \tag{1}$$

a final state X is produced, while the nuclei normally remain in their ground state.

These reactions occur through the collision of two exchange particles. For purely electromagnetic interactions, the exchange particles are photons, and the process corresponds to a two-photon interaction. For the strong nuclear force, the exchange particles are in principle gluons. Gluons cannot, however, couple coherently to several nucleons, since they have a color charge. The colorless exchange particle of the nuclear interaction is the

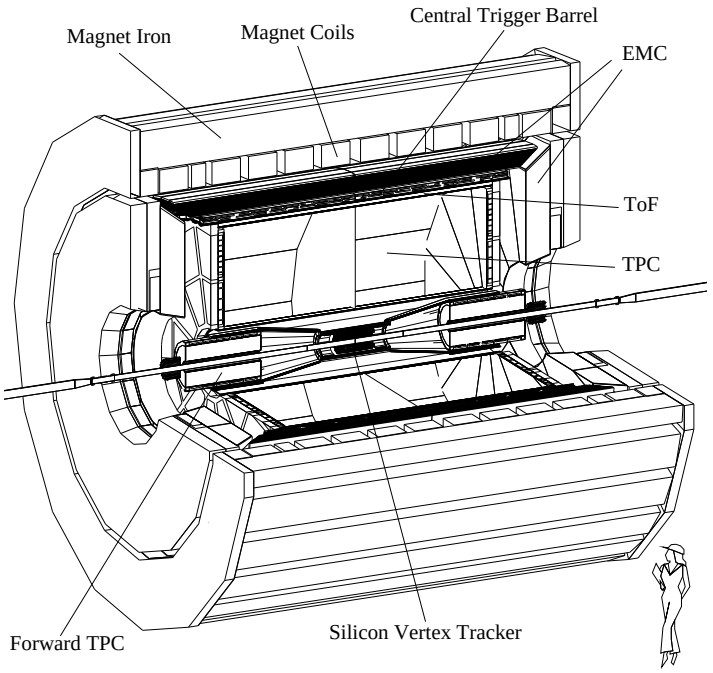

Figure 1: The STAR detector at RHIC. The outer radius of the TPC cylinder is 2 m and the length is 4 m.

Pomeron, which, under certain circumstances, might be interpreted as a pair of gluons or a gluon ladder[3]. Colorless nuclear interactions may also be mediated by mesons. Coherent nuclear interactions can thus be of the following types: two–photon, photon-Pomeron/meson (photonuclear) and Pomeron/meson–Pomeron/meson. The cross section for Pomerom–Pomeron reactions is expected to be low[4]. In the rest of this paper, only two-photon and photonuclear interactions will be discussed further.

The maximum 4–momentum transfer in a coherent nuclear interaction is determined by the nuclear form factor. The maximum momentum transfer for coherence is $Q_{max} \sim \hbar c/R$ in the rest frame of the nucleus, where R is the nuclear radius. This has two important consequences. First, the transverse momentum of the final state is limited to $p_T \leq \sqrt{2}\hbar c/R$. Secondly, the maximum photon energy is limited to $\gamma\hbar c/R$, where γ is the Lorentz factor of the nucleus in the relevant frame.

The flux of virtual photons from the electromagnetic field of the nuclei scales as Z^2, so the two-photon luminosity scales as Z^4. This is one of the advantages of studying two–photon interactions in nuclear collisions. For Pomerons/mesons the scaling with A is more complicated because of nuclear shadowing, as will be discussed in the section on photonuclear interactions.

The maximum two-photon center–of–mass energy is $\sim 2\gamma\hbar c/R$, where γ is the Lorentz factor of the nuclei in the center–of–mass frame. This is about 6 GeV for heavy nuclei at RHIC. RHIC will be the first accelerator energetic enough to produce hadronic final states in coherent interactions.

3 Two-Photon Interactions

Two–photon interactions at RHIC will have energies in the region dominated by resonance production. Neutral resonances with spin J=0 or 2 can be produced in a collision of two

quasi–real photons. Meson pairs ($\pi^+\pi^-$, $\pi^0\pi^0$, K^+K^- etc.) and lepton pairs (e^+e^-, $\mu^+\mu^-$, $\tau^+\tau^-$) can also be produced. A few of the very many interesting physics topics that can be studied in two–photon collisions at RHIC are the following:

Electron/Lepton pair production: Reactions of the type $Au + Au \rightarrow Au + Au + e^+e^-$. The calculation of the cross section for this process has attracted some interest recently[5, 6, 7, 8]. The process is pure QED, but $Z\alpha \sim 0.6$. Calculations using first order perturbation theory violates unitarity (the interaction probability becomes larger than 1) even at fairly large impact parameters ($b \sim \lambda_C = 386$ fm)[9]. Unitarity can be restored if higher order terms are included in the calculations[10]. These higher order terms lead to the production of multiple pairs. The importance of higher order effects is still under debate. Recent non–perturbative calculations have found that the e^+e^- cross section is identical to that obtained from lowest–order perturbation theory[6]. Non–perturbative effects should be present in the production of multiple pairs. These results were criticized in Ref. [5], which concluded that higher order terms contribute 25% of the e^+e^- cross section at RHIC. Measurements of single and multiple electron/positron pairs should help resolving these theoretical difficulties and serve as a probe of strong–field QED.

Meson Spectroscopy: Reactions of the type $\gamma\gamma \rightarrow$ Resonance can be used to probe the quark content of the produced state. Photons couple to charge, $\Gamma_{\gamma\gamma} \propto Q^4$. A nice illustration of this is the two–photon widths of the neutral mesons ($f_2(1270)$, $a_2(1320)$, and $f_2'(1525)$) in the tensor meson nonet. These states are believed to have the quark compositions shown below.

Meson	Quark Composition	$\Gamma\gamma\gamma$(relative)	$\Gamma\gamma\gamma$(measured)
$f_2(1270)$	$\frac{1}{\sqrt{2}}\|u\overline{u} + d\overline{d}>$	25	2.8 keV
$a_2(1320)$	$\frac{1}{\sqrt{2}}\|u\overline{u} - d\overline{d}>$	9	1.0 keV
$f_2'(1525)$	$\|s\overline{s}>$	2	0.1 keV

From this one can easily compute the expected relative two–photon width. As can be seen, this is also in good agreement with the measured values.

For a pure glueball, $\Gamma_{\gamma\gamma} = 0$ to first order and the cross section for two-photon production would vanish. Stringent limits on the two–photon widths is an important test for glueball candidates. Two of the most promising glueball candidates are the $f_0(1500)$[11] and the $f_J(2220)$ (also known as $\xi(2230)$)[12].

Meson Pair Production: At the hadron level, photons couple only to charged mesons. So, $\pi^+\pi^-$ should be produced, with $\pi^0\pi^0$ suppressed. This picture applies near threshold, where the photon wavelength is large compared to the size of the meson. However, at higher energies, the photons 'see' and couple to quarks and $\pi^+\pi^-$ and $\pi^0\pi^0$ are produced in comparable numbers. By comparing the rates of the two final states, the transition can be studied, and the size of the mesons determined.

However, for some channels, other mechanisms may apply. The reaction $\gamma\gamma \rightarrow \rho^0\rho^0$ is of special interest. A resonance is observed near threshold for $M_{\rho\rho} \sim 1.3 - 1.6$ GeV. A similar resonance is not observed in the $\rho^+\rho^-$ channel[13].

The cross section for the two–photon production of a state is usually factorized into a cross section for $\gamma\gamma$ fusion and an equivalent $\gamma\gamma$ luminosity,

$$\sigma(A + A \rightarrow A + A + X) = \int\int \frac{d\mathcal{L}_{\gamma\gamma}}{dWdY}\sigma_{\gamma\gamma\rightarrow X}(W)dWdY \ . \qquad (2)$$

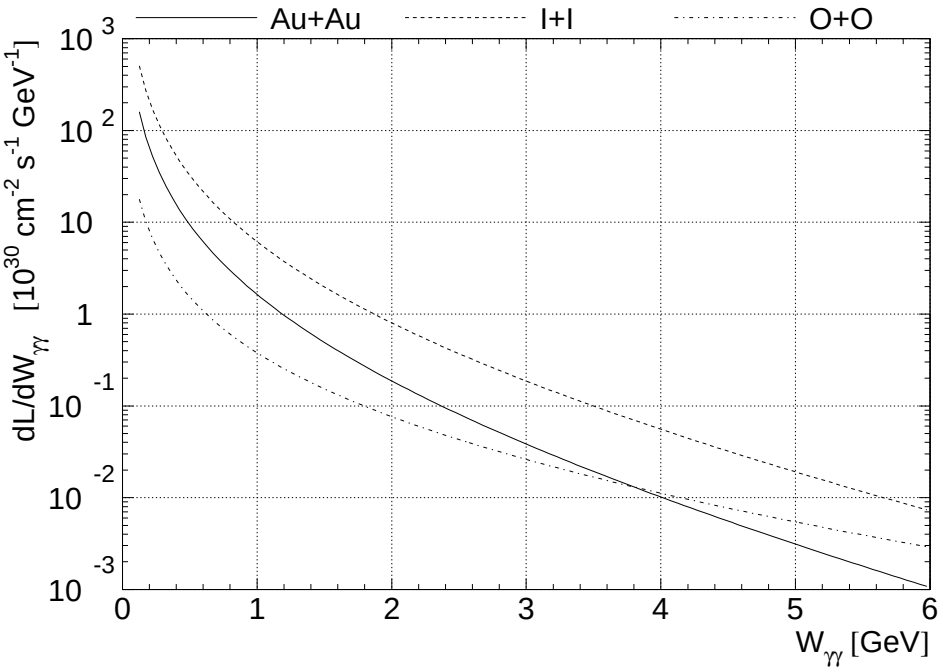

Figure 2: Differential two–photon luminosity, $d\mathcal{L}/dW$, for O+O, I+I, and Au+Au collisions at RHIC.

The two–photon cross sections, $\sigma_{\gamma\gamma\to X}(W)$, for single resonances, lepton and meson pairs can be found in Ref. [14].

The two–photon luminosity in peripheral nucleus–nucleus collisions has been discussed by several authors [15]. These analyses use the Weizsäcker–Williams method in the impact parameter representation to calculate the equivalent photon flux. When the nuclear impact parameter, b, is smaller than the sum of the nuclear radii, hadronic interactions will dominate. To find the usable two-photon luminosity this region must be excluded from the integration. In the papers cited above, this is accomplished by introducing a sharp cut of at $b = R_1 + R_2$. The differential luminosity is

$$\frac{d\mathcal{L}_{\gamma\gamma}}{d\omega_1 d\omega_2} = \mathcal{L}_{AA} \int_{b_1>R} \int_{b_2>R} n(\omega_1, b_1) n(\omega_2, b_2) \Theta(\mid \vec{b}_1 - \vec{b}_2 \mid -2R) d^2b_1 d^2b_2 \ , \tag{3}$$

where $n(\omega, b)$ is the Weizsäcker–Williams photon flux from one of the nuclei at a distance b from its center. The Θ–function is defined as $\Theta(x) = 0$ for $x < 0$ and $\Theta(x) = 1$ for $x > 0$. Then, for $\gamma \gg 1$,

$$n(\omega, b) = \frac{dN}{d\omega d^2b} = \frac{Z^2\alpha}{\pi^2} \frac{1}{\omega b^2} x^2 K_1^2(x) \ . \tag{4}$$

Here, ω is the photon energy, b the impact parameter, and $x = b\omega/\gamma$ [16]. In Eq. 4 and in the rest of this paper, natural units are used, i.e. $\hbar = c = 1$. Since $n(\omega, b) \sim Z^2$, the luminosity essentially scales as Z^4. The scaling is inexact, however, because of the Θ-function in Eq. 3 and the variation of R with A/Z.

A variable transformation from the individual photon energies, ω_1 and ω_2, to the $\gamma\gamma$ center–of–mass energy, W, and rapidity, Y, is achieved by

$$\begin{array}{rclcrcl} \omega_1 &=& \frac{1}{2} W e^{Y} & & W &=& \sqrt{4\omega_1\omega_2} \\ \omega_2 &=& \frac{1}{2} W e^{-Y} & & Y &=& \frac{1}{2}\ln(\omega_1/\omega_2) \ . \end{array} \tag{5}$$

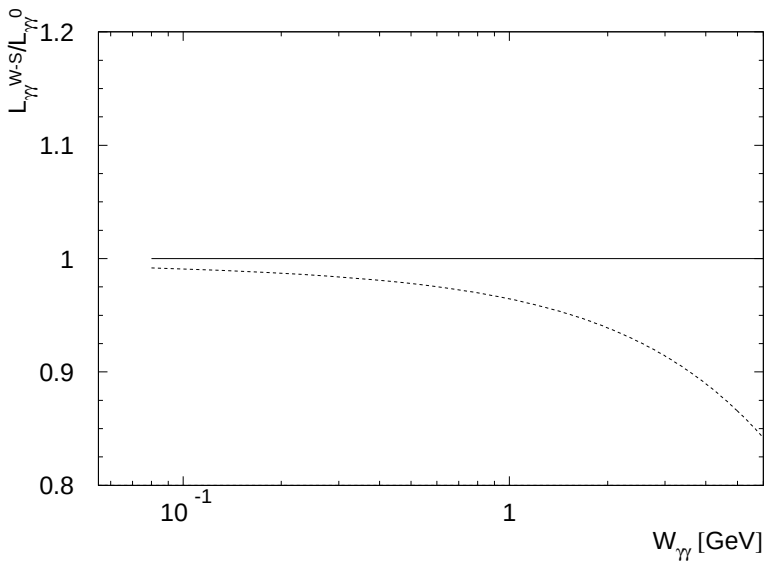

Figure 3: Reduction in two–photon luminosity when the nucleon density is approximated with a Woods–Saxon distribution (dotted line) as compared with a flat distribution for $r < R_{nuc}$ (solid line). The calculation is for gold–gold interactions at 100+100 A GeV.

The differential $\gamma\gamma$ luminosity, $d\mathcal{L}_{\gamma\gamma}/dW$, is then

$$\frac{d\mathcal{L}_{\gamma\gamma}}{dW} = \int_{-\infty}^{\infty} \frac{d\mathcal{L}_{\gamma\gamma}}{dW dY} dY \ . \tag{6}$$

Figure 2 shows the equivalent two–photon luminosity for three different nuclear systems at RHIC, calculated from Eq. 3. The highest two–photon luminosity is obtained in I+I interactions. The lower Z is compensated by higher nuclear luminosity and smaller nuclear radius.

The sharp cut–off at $b = 2R$ in Eq. 3 treats the nuclei as hard spheres. In a more realistic model one has to consider also the diffuseness of the nuclear surface. This can be accomplished by first rewriting the expression for the luminosity as

$$\frac{d\mathcal{L}_{\gamma\gamma}}{d\omega_1 d\omega_2} = \mathcal{L}_{AA} \int_{b_1>R} \int_{b_2>R} n(\omega_1, b_1)\, n(\omega_2, b_2)\, [\, 1 - P_{INT}(\mid \vec{b}_1 - \vec{b}_2 \mid)\,]\, d^2b_1 d^2b_2 \ . \tag{7}$$

where $P_{INT}(b)$ is the hadronic interaction probability for a nucleus–nucleus collision at impact parameter b. There is a finite probability for having an interaction also at impact parameters $b > 2R$. This probability can be calculated using the Glauber Model:

$$P(b) = 1 - \exp\left(-\sigma_{nn} \int T_A(r) T_B(b-r) d^2r\right) \tag{8}$$

where σ_{nn} is the hadronic nucleon–nucleon cross section and $T(r)$ is the nuclear thickness function[17]. Here, $\sigma_{nn} = 52$ mb is used, corresponding to $\sqrt{s}$=200 GeV [13]. The thickness function is calculated from the nucleon density distribution ρ,

$$T(\vec{b}) = \int \rho(\vec{b}, z) dz \ . \tag{9}$$

For ρ, a Woods–Saxon or Fermi distribution is used:

$$\rho(r) = \frac{\rho_0}{1 + \exp(\frac{r - R_{nuc}}{c})} \ . \tag{10}$$

Final State	$\Gamma_{\gamma\gamma}$	Au+Au		I+I	
	[keV]	σ [μb]	Evts./Year	σ [μb]	Evts./Year
π^0	7.8 eV	4700	$9.4 \cdot 10^6$	1100	$3.0 \cdot 10^7$
η	0.5	884	$1.8 \cdot 10^6$	229	$6.2 \cdot 10^6$
η'	4.3	642	$1.3 \cdot 10^6$	178	$4.8 \cdot 10^6$
$f_0(980)$	0.6	75	$1.5 \cdot 10^5$	21	$5.6 \cdot 10^5$
$f_2(1270)$	2.8	514	$1.0 \cdot 10^6$	149	$4.0 \cdot 10^6$
$a_2(1320)$	1.0	155	$3.1 \cdot 10^5$	45	$1.2 \cdot 10^6$
$f_2'(1525)$	0.1	7	$1.4 \cdot 10^4$	2	$5.8 \cdot 10^4$
$\eta_c(2980)$	7.5	2	$4.7 \cdot 10^3$	1	$2.3 \cdot 10^4$
$\mu^+\mu^-$	–	130 mb	$2.7 \cdot 10^8$	33 mb	$8.9 \cdot 10^8$
$\tau^+\tau^-$	–	0.65	$1.3 \cdot 10^3$	0.29	$8.0 \cdot 10^3$
$\rho^0\rho^0$	–	20	$4.0 \cdot 10^4$	6	$1.6 \cdot 10^5$

Table 2: Cross sections and production rates at RHIC for various final states in two–photon interactions at design luminosity. One year corresponds to 10^7 seconds of operation. The $\rho^0\rho^0$ is in the invariant mass range 1.5–1.6 GeV.

where R_{nuc} is the nuclear radius and c is the skin–thickness. Here, the radius is calculated from $R_{nuc} = r_0 A^{1/3}$ with $r_0 = 1.16(1. - 1.16A^{-2/3})$ fm, and a constant skin–thickness of c=0.53 fm is used. These parameterizations are obtained from electron–nucleus scattering data[18].

The effect of using a Woods–Saxon distribution for the nucleon density as compared with a Θ–function is shown by the dotted curve in Fig. 3. The luminosity is reduced up to 15%, depending on energy.

The cross sections and production rates (using a Woods–Saxon distribution) for various resonances, muon and tau pairs, and $\rho\rho$ pairs are shown in Table 2 for Au+Au and I+I interactions. For mesons in the mass range 0–2 GeV, the production rates will be between 10^5–10^7 events per year. In section 5 these rates will be compared with the rates of background reactions.

4 Photonuclear Interactions

In this section exclusive vector meson production in photonuclear interactions will be discussed. These reactions are of the type $\gamma + A \to V + A$, where V is a vector meson (ρ, ω, ϕ and J/Ψ are discussed here). The reactions are usually described within the framework of the Vector Dominance Model and are assumed to proceed in the following way: One of the nuclei emits a photon, which fluctuates into a vector meson. The vector meson then scatters off the other nucleus.

There are several reasons to study these interactions in nuclear systems. The reaction $\gamma + N \to V + N$ (N is a nucleon) is mediated by mesons (dominant at low energy) and by Pomerons (dominant at high energy). By extending these studies to nuclei one can study how Pomerons and mesons couple to nuclei.

Photonuclear J/Ψ production is of special interest since in photonucleon interactions the energy dependence violates the soft–Pomeron/Regge-theory behaviour. It has been suggested that the diffractive production of J/Ψ–mesons on nuclear targets can probe the gluon distributions in nuclei[19, 20].

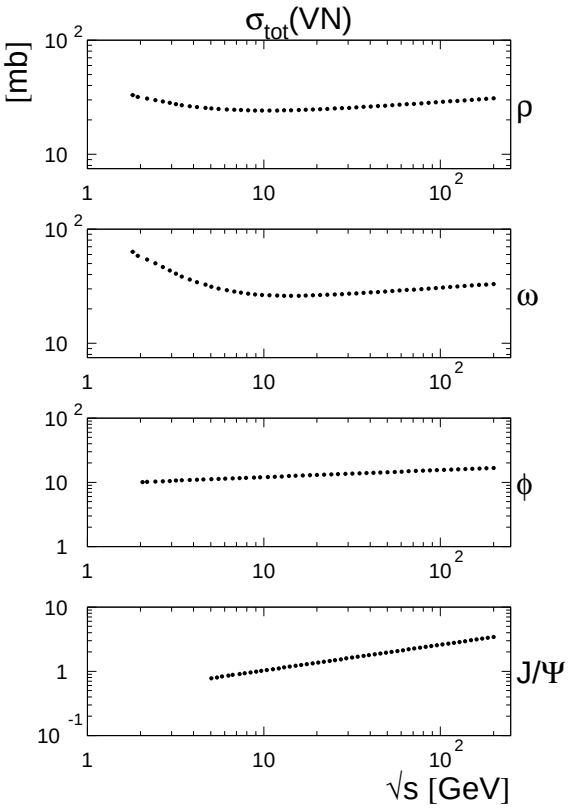

Figure 4: Total inelastic vector meson–nucleon cross sections.

The cross section for the exclusive production of one vector meson is calculated as the product of the Weizsäcker–Williams photon flux, $n(\omega)$, with the photonuclear cross section, $\sigma_{\gamma A}$, integrated over photon energy,

$$\sigma(A + A \to A + A + V) = 2 \int \sigma_{\gamma A \to V A}(\omega)\, n(\omega)\, d\omega \; . \tag{11}$$

The factor of 2 is because either nucleus can emit a photon. The photon flux is calculated by integrating Eq. 4 over all impact parameters $b > 2R$, and averaging over the area of the target nucleus[21].

The 4–momentum transfer from the target nucleus, t, will be determined by the nuclear form factor, $F(t)$, in coherent reactions. The cross section is

$$\sigma_{\gamma A}(E_\gamma) = \int_{t_{min}}^{\infty} \left. \frac{d\sigma}{dt} \right|_{t=0} |F(t)|^2 \, dt \; . \tag{12}$$

$F(t)$ can be approximated with a gaussian,

$$F(t) = e^{-|t|/2Q_0^2} \; . \tag{13}$$

For a gold nucleus $Q_0 = 60$ MeV [22]. In the narrow width approximation ($\Gamma_V = 0$), $t_{min} = [M_V^2/4\omega\gamma]^2$. A more realistic model includes the natural width of the vector meson (important for the ρ)[23].

The forward scattering amplitude is extrapolated from γN interactions. Studies at the electron–proton collider HERA have shown that the cross section for exclusive vector meson production at high energies increases slowly with energy. The variation is consistent

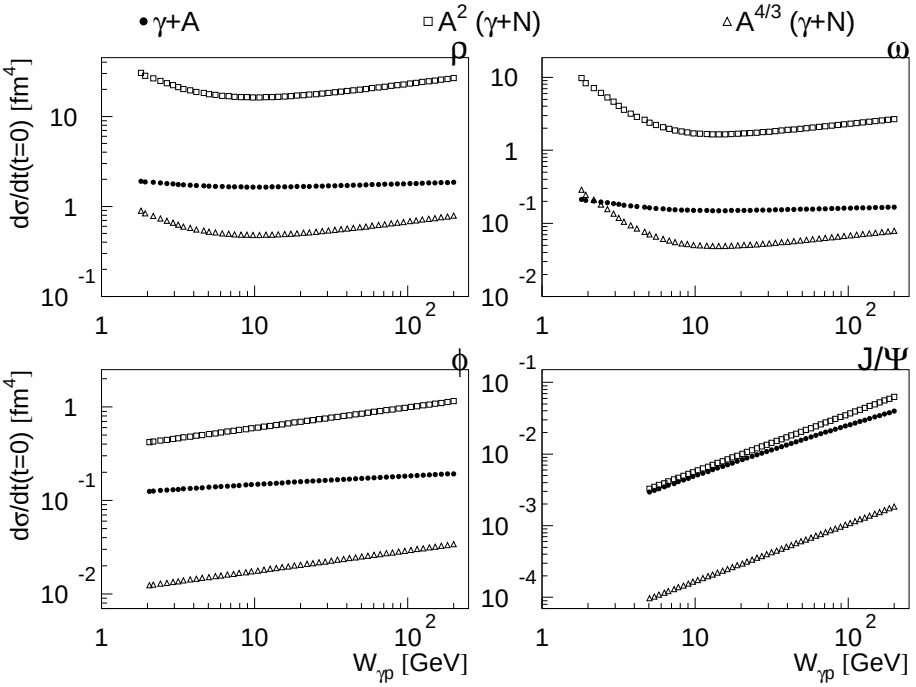

Figure 5: Forward scattering amplitudes for diffractive vector meson production on gold nuclei.

with Regge theory and soft–Pomeron exchange. Exclusive vector meson production is summarized in Ref. [24], from which the following parameterization can be extracted:

$$\sigma(\gamma p \to V p) \;=\; X\, w_{\gamma p}^{\epsilon} \;+\; Y\, w_{\gamma p}^{-\eta}\;, \tag{14}$$

where $w_{\gamma p}$ is the γp center–of–mass energy (in GeV). The values of X, Y, ϵ, and η are given in Table 3. For ϕ and J/Ψ the cross section rises monotonically with s and only the first term in Eq. 14 is necessary. For these mesons only Pomeron exchange contribute[25], while for the ρ and ω meson exchange dominates at low energies.

The t dependence can be parameterized as [24, 26]

$$\frac{d\sigma}{dt} = \left.\frac{d\sigma}{dt}\right|_{t=0} e^{-b|t|+c|t|^2}\;. \tag{15}$$

The constant c is small, and the behaviour is essentially exponential. To simplify the following calculations, it will be assumed that $c = 0$. The forward scattering amplitude is then

$$\left.\frac{d\sigma}{dt}\right|_{t=0} = b \cdot (X\, w_{\gamma p}^{\epsilon} + Y\, w_{\gamma p}^{-\eta})\;. \tag{16}$$

Meson	$f_v^2/4\pi$	X [μb]	ϵ	Y [μb]	η	b [GeV^{-2}]
ρ^0	2.02	5.0	0.22	26.0	1.23	11
ω	23.13	0.55	0.22	18.0	1.92	10
ϕ	13.71	0.34	0.22	–	–	7
J/Ψ	10.45	0.0015	0.80	–	–	4

Table 3: Photon–vector meson couplings and parameterizations of the vector meson cross sections. The vaules for b are from Ref. [24]. See text for details.

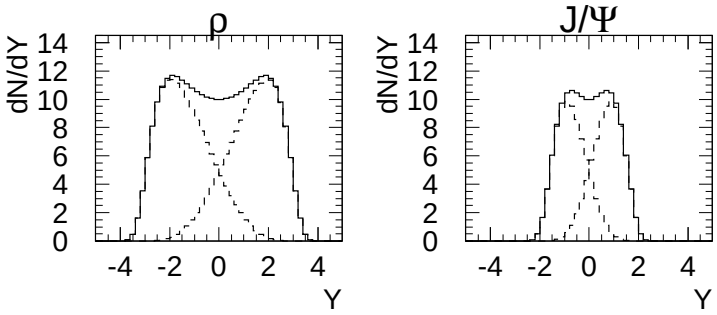

Figure 6: Rapidity distributions of ρ and J/Ψ mesons produced in exclusive reactions $Au + Au \rightarrow Au + Au + V$. The total distribution (solid histogram) is the sum of the distributions for photon scattering off each of the projectile nuclei (dashed histograms).

In Vector Meson Dominance, the forward scattering amplitude for the reaction $\gamma + N \rightarrow V + N$ is given by the forward scattering amplitude for elastic $V + N$ scattering times the γ–vector meson coupling. The coupling is related to the width for the decay into an e^+e^- pair,

$$\frac{f_v^2}{4\pi} = \frac{1}{3}\frac{m_v \alpha^2}{\Gamma_{V\rightarrow e^+e^-}} \; , \tag{17}$$

where m_v is the vector meson mass[27]. Using the values of $\Gamma_{V\rightarrow e^+e^-}$ in Ref. [13], the couplings in Table 3 are obtained. Eq. 17 is modified slightly when higher vector meson states are taken into account (Generalized Vector Meson Dominance Model), but this is not considered here. The total inelastic vector meson–nucleon cross section can then be related to the forward scattering amplitude by the optical theorem,

$$\frac{\sigma_{tot}^2}{16\pi} = \frac{f_v^2}{4\pi\alpha}\left.\frac{d\sigma}{dt}\right|_{t=0} (\gamma N \rightarrow VN) \; . \tag{18}$$

The inelastic cross sections obtained from this are shown in Fig. 4. The cross sections for ρ and ω are of the same order of magnitude as those for π–nucleon scattering, whereas the cross section for ϕ– and J/Ψ–nucleon scattering are smaller.

The total inelastic cross sections determine the scaling of $d\sigma/dt$ when going from γ–nucleon to γ–nucleus scattering through the optical theorem:

$$\frac{d\sigma/dt|_{t=0}\,(\gamma A \rightarrow VA)}{d\sigma/dt|_{t=0}\,(\gamma N \rightarrow VN)} = \frac{\sigma_{tot}^2(VA)}{\sigma_{tot}^2(VN)} \tag{19}$$

The total inelastic vector meson–nucleus cross sections are calculated from the inelastic cross sections for vector meson–nucleon scattering using the Glauber Model (cf. Eqs. 8 and 9):

$$\sigma_{tot}(VA) = \int (1 - e^{-\sigma(VN)T(b)}) d^2b \; . \tag{20}$$

The resulting forward scattering amplitudes are plotted in Fig. 5. The calculated values for γ-nucleus scattering are compared with a simple $A^{4/3}$ and A^2 scaling of the

corresponding value for γ–nucleon scattering. The scaling A^2 corresponds to weak absorption (σ_{VN} small), and $A^{4/3}$ corresponds to strong "black disc" absorption (σ_{VN} large). For the ρ and the ω, the scaling is closest to $A^{4/3}$. For the J/Ψ nuclear shadowing is less important because of the much smaller inelastic cross section, and the scaling is close to A^2. The ϕ shows more shadowing than the J/Ψ but less than the lighter mesons. The unit for $d\sigma/dt$ is [μb GeV^{-2}]. For simplicity, this has been converted to [fm^4] in the figure.

The cross sections for gold–gold interactions are listed in Table 4. The table also lists the corresponding production rates at the design luminosity. Both the cross sections and production rates are high. The cross section for diffractive ρ–meson production is roughly 10% of the total inelastic Au+Au cross section. The rates are higher than for most two–photon final states.

The rapidity distributions for ρ and J/Ψ final states are shown in Fig. 6. The narrower distribution for the J/Ψ is a kinematical effect caused by the higher mass of the J/Ψ.

Meson	σ [mb]	Prod. Rate [Hz]
ρ^0	640	130
ω	60	12
ϕ	41	8
J/Ψ	320 μb	6.5 $\cdot 10^{-2}$

Table 4: Cross sections and production rates for exclusive vector meson production in Au+Au interactions.

5 Experimental Techniques

Two–photon and coherent photonuclear interactions have never been studied in heavy–ion collisions before. To be able to study them it is necessary to develop adequate triggering and analysis techniques. This section will discuss the experimental procedures that have been developed for the STAR experiment.

It will not be possible to tag the outgoing nuclei, because the typical transverse momentum transfers ($\approx$ 30 MeV for Au) are completely negligible compared with the total energy of the nuclei (19.7 TeV for Au); the resulting angular deflections will be of the order of microradians. Other techniques must be used to separate the coherent interactions from background processes.

The analysis is based on using the characteristics of coherent events and developing cuts that reject as much of the background as possible. It is assumed that the entire final state is detected and that no other particles are present in the event. The following variables are used:

1. Charged Particle Multiplicity: The resonances formed in two–photon interactions decay into final states with low multiplicity (2 or 4 charged particles for the states studied here).
2. Charge Conservation: Since no charge exchange occur the final state is required to obey $\sum Q_i = 0$.
3. FTPC Multiplicity: It is required that the entire event is detected in the main TPC. By rejecting events with tracks in the forward TPCs backgrounds are reduced.

4. Final State Rapidity: Two–photon events are centered around midrapidity with a fairly narrow width. Requiring $|y_{cm}| < 0.75$ reduces the background, particularly from beam–gas and incoherent photonuclear interactions, with little loss of signal.
5. Transverse Momentum: Coherent events will have $p_T \sim 1/R$. Cuts on the transverse momenta of $p_T \leq 100$ MeV/c and $p_T \leq 50$MeV are used for triggering and off–line analysis, respectively.

Two–photon events have been generated with the STARLight Monte Carlo[29]. The geometrical acceptance of the main TPC has been conservatively defined as $|\eta| < 1.5$ and $p_T > 150$ MeV with 100% detection efficiency. For the forward TPC the corresponding cuts are $2.5 \leq| \eta |\leq 3.75$ and $p_T > 100$ MeV/c.

The following sources of backgrounds have been identified: peripheral (hadronic) nucleus–nucleus collisions, beam–gas interactions, upstream interactions, photonuclear interactions (incoherent), and cosmic rays. The backgrounds have been simulated with different Monte Carlo codes. For hadronic nucleus–nucleus collisions and beam–gas events, FRITIOF 7.02[30] and VENUS 4.12[31] have been used. Photonuclear events have been simulated with DTUNUC 2.0[32]. For cosmic rays (muons) HemiCosm[33] has been used. Details of these simulations are given in Ref. [28]. Here, the general techniques will be described together with the current best background estimates. The simulations are focussed on two–photon final states. The backgrounds to photonuclear events have not been studied in detail yet. However, because of the similar kinematics, the backgrounds are expected to be similar to $\gamma\gamma$ reactions, while the signals are considerably higher. Simulations have been performed both for the trigger and the off–line analysis. The trigger will be considered first.

The STAR trigger has 4 levels (0, 1, 2, and 3). Levels 1 and 2 are combined here because it is not clear what calculations are possible in Level 1 and what will have to wait until Level 2. Level 0 uses programmable logic to determine the multiplicity in $\sim 2\mu s$. Inputs are the CTB and the TPC wire multiplicity, $|\eta| < 2$. Levels 1 and 2 use the same information, processed by a computer for more accurate multiplicity information (e.g. merging adjacent hits). TPC tracking will be available in Level 3, after approximately 10 ms.

In Level 0 a multiplicity cut of $2 \leq n_{ch} \leq 5$ is applied in combination with a crude topology cut (back–to–back in ϕ). For Levels 1/2 the multiplicity cut is sharpened to $n_{ch} = 2$ or 4, and it is required that there are no tracks in the region $1.5 < |\eta| < 2.0$. Level 3 requires $p_T \leq 100$ MeV/c and the vertex is required to be within the reaction diamond. The background trigger rates after these cuts have been applied are shown in Table 5. Even at Level 1/2 these background rates are less than the signal rates from photonuclear interactions. The rates are well within the capabilities of the STAR trigger system.

Trigger	Hadronic A+A		Beam–Gas		γ+A	Cosmic Rays	Total
Level	FRITIOF	VENUS	FRITIOF	VENUS	DTUNUC	HemiCosm	Rate
0	18	21	53	53	63	26	160
1/2	2	4	6	7	11	18	38
3	0.03	0.1	0.1	0.1	0.6	0.4	1.2

Table 5: Trigger Rates (in Hz) of the various background processes discussed in the text for gold–beams at the design luminosity.

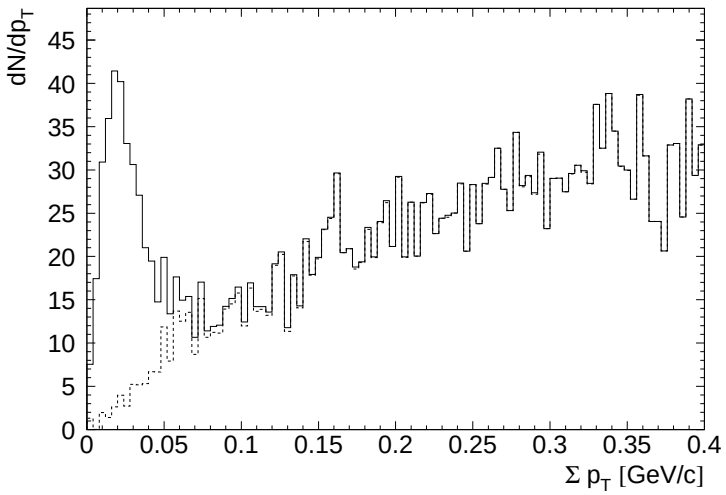

Figure 7: Transverse momentum distribution for $\gamma\gamma \to f_2(1270) \to \pi^+\pi^-$ and backgrounds. The solid histogram shows the signal plus backgrounds and the dashed histogram shows the backgrounds.

Detailed analyses have been performed for the following three systems: one intermediate mass meson, $f_2(1270) \to \pi^+\pi^-$; one meson pair, $\rho\rho \to \pi^+\pi^-\pi^+\pi^-$; and one heavy meson, $\eta_c(2980) \to K^+\pi^-K^-\pi^+$. These systems are representative of a wide selection of two–photon final states.

The production rates for these states are shown in Table 2. Taking into account the branching ratios for the decay modes studied and the geometrical acceptance of STAR gives the rates shown on the first line in Table 6. Applying the cuts 1–5 for the peripheral collisions analysis above gives the rates shown on the second line of the same table. A similar analysis was made on the background events generated with FRITIOF/VENUS/DTUNUC, and the results are shown in the table. For the backgrounds, suitable cuts have been applied on the invariant mass. As an illustration, the effect on the transverse momentum distribution of the cuts 1–4 above is shown in Figure 7.

As can be seen, the signal to noise ratio will be very high for $f_2(1270)$ and ρ–pairs. For the η_c particle identification (separation of pions from kaons) is necessary in order to suppress the backgrounds sufficiently.

	System		
	$f_2(1270)$	$\rho^0\rho^0$	$\eta_c(2980)$
Within STAR Acceptance	380,000	9,500	33
After analysis cuts	300,000	8,500	30
Peripheral AA (FRITIOF/VENUS)	400/4,000	50/460	90/680
Beam–gas (FRITIOF/VENUS)	400/1,000	6/6	<1/<1
γ+A (DTUNUC)	15,000	1,000	730
Background without PID	16,000/20,000	1,000/1,500	820/1,400
Background with PID			9/15

Table 6: Estimated signal and background rates (Events/year) with and without particle identification, for two–photon production of $f_2(1270)$, $\rho^0\rho^0$ and $\eta_c(2980)$ in Au+Au collisions.

6 Conclusions

RHIC will be the first heavy–ion accelerator energetic enough to produce final states with masses of several GeV in coherent interactions. This will provide an opportunity for the study of many interesting physics topics. Some of these, e.g. strong–field multiple e^+e^-–pair and coherent vector meson production, are unique to heavy–ion colliders.

The rates for coherent two–photon and photonuclear interactions have been calculated and are found to be high. The experimental feasibility of studying these interactions have been demonstrated. Analysis techniques and algorithms have been developed which allow the separation of signal from background.

Acknowledgements

J.N. would like to thank the organizers for the invitation to give a talk at this enjoyable conference at his *Alma Mater*. This work was supported by the U.S. DOE under contract DE–AC–03–76SF00098.

References

[1] Conceptual Design of the Relativistic Heavy Ion Collider, BNL–52195 (Brookhaven National Laboratory, May 1989).

[2] STAR Collaboration, Conceptual Design Report for the Solenoidal Tracker at RHIC, LBL PUB–5347, June 1992.

[3] Quantum Chromodynamics and the Pomeron, J.R. Forshaw and D.A. Ross (Cambridge University Press, 1997).

[4] A.J. Schramm and D.H. Reeves, Phys. Rev. **D 55** (1997) 7312.

[5] D.Yu. Ivanov, A. Schiller, and V.G. Serbo, hep–ph/9809281.

[6] A.J. Baltz and L. McLerran, Phys. Rev. **C 58** (1998) 1679; B. Segev and J.C. Wells, Phys. Rev. **A 57** (1998) 1849; U. Eichmann, J. Reinhardt, and W. Greiner, nucl–th/9806031; U. Eichmann, J. Reinhardt, S. Schramm, and W. Greiner, nucl–th/9804064 (to appear in Phys. Rev. **A**).

[7] A. Alscher, K. Hencken, D. Trautmann, and G. Baur, Phys. Rev. **A 55** (1997) 396.

[8] K. Hencken, D. Trautmann, and G. Baur, Phys. Rev. **A 51** (1995) 998; *ibid.* **A 51** (1995) 1874.

[9] C.A. Bertulani and G. Baur, Phys. Rep. **163** (1988) 299.

[10] G. Baur, Phys. Rev. **A 42** (1990) 5736.

[11] ALEPH Collaboration, Proc. EPS–HEP Conference, Jerusalem, August 1997.

[12] CLEO Collaboration, R. Godang *et al.*, Phys. Rev. Lett. **79** (1997) 3829.

[13] Particle Data Group, Review of Particle Physics, C. Caso *et al.* Eur. Phys. J. **C 3** (1998) 1.

[14] S.J. Brodsky, T. Kinoshita, and H. Terazawa, Phys. Rev. **D 4** (1971) 1532.

[15] G. Baur and L.G. Ferreira Filho, Nucl. Phys. **A 518** (1990) 786; R.N. Cahn and J.D. Jackson, Phys. Rev. **D 42** (1990) 3690; M. Vidovic, M. Greiner, C. Best, and G. Soff, Phys. Rev. **C 47** (1993) 2308; K. Hencken, D. Trautmann, and G. Baur, Z. Phys. **C 68** (1995) 473. See also G. Baur, these proceedings.

[16] Classical Electrodynamics, J.D. Jackson (John Wiley & Sons, 1975).

[17] R.J. Glauber in Lectures in Theoretical Physics, Eds. W.E. Brittin and L.G. Dunham (Interscience, New York, 1959); C.Y. Wong, Introduction to High–Energy Heavy–Ion Collisions (World Scientific, 1994).

[18] Nuclear Sizes and Structure, R.C. Barrett and D.F. Jackson (Oxford University Press, 1977).

[19] S.J. Brodsky *et al.*, Phys. Rev. **D 50** (1994) 3134.

[20] M.G. Ryskin, R.G. Roberts, A.D. Martin, and E.M. Levin, Z. Phys. **C 76** (1997) 231.

[21] N. Baron and G. Baur, Phys. Rev. **C 48** (1993) 1999.

[22] M. Drees, J. Ellis, and D. Zeppenfeld, Phys. Lett. **B 223** (1989) 454.

[23] S. Klein and J. Nystrand, in preparation.

[24] Exclusive Production of Neutral Vector Mesons at the Electron–Proton Collider HERA, J.A. Crittenden (Springer–Verlag, 1997).

[25] P.G.O. Freund, Nuovo Cimento **A 48** (1967) 541.

[26] ZEUS Collaboration, J. Breitweg *et al.*, Eur. Phys. J. **C 2** (1998) 247.

[27] A. Donnachie and G. Shaw, in Electromagnetic Interactions of Hadrons, Eds. A. Donnachie and G. Shaw (Plenum Press, 1978), Vol. 2, p. 169.

[28] S. Klein and J. Nystrand, STAR Note 347, June 1998, available on the WWW at http://rsgi01.rhic.bnl.gov/star/starlib/doc/www/sno/ice/sn0347.html.

[29] S. Klein and E. Scannapieco, in Proc. Photon '97, Egmond aan Zee, The Netherlands, May 10–15, 1997, Eds. A. Buijs and F.C. Berné (World Scientific, 1998), p. 348. hep–ph/9706358.

[30] H. Pi, Comp. Phys. Comm. **71** (1992) 173.

[31] K. Werner, Phys. Rep. **232** (1993) 87.

[32] R. Engel, J. Ranft, and S. Roesler, Phys. Rev. **D 55** (1997) 6957; *ibid.* **D 57** (1998) 2889.

[33] M.P. Bringle, BaBar Note 163 (1994) (unpublished).